Journal of Power Sources 212 (2012) 179–185

Contents lists available at SciVerse ScienceDirect

Journal of Power Sources

journal homepage: www.elsevier.com/locate/jpowsour

Lithium-sulfur cell with combining carbon nanofibers–sulfur cathode and gel polymer electrolyte

Mumin Rao [a,b], Xiuyu Geng [a], Xiaoping Li [a], Shejun Hu [a], Weishan Li [a,b,*]

[a] School of Chemistry and Environment, South China Normal University, Guangzhou 510006, China
[b] College of Materials Science and Engineering, South China University of Technology, Guangzhou 510641, China

ARTICLE INFO

Article history:
Received 30 November 2011
Received in revised form
25 February 2012
Accepted 14 March 2012
Available online 16 April 2012

Keywords:
Sulfur
Carbon nanofiber
Gel polymer electrolyte
Electrospun poly(acrylonitrile)/poly(methyl methacrylate)
Lithium-sulfur cell

ABSTRACT

In this paper we report a novel lithium-sulfur cell, which is characteristic of a unique combination of carbon nanofibers–sulfur cathode and gel polymer electrolyte (GPE). In particular, the carbon nanofibers for the cathode and the poly(acrylonitrile)/poly(methyl methacrylate) (PAN/PMMA) membrane for the GPE are prepared by electrospinning technique. The GPE consists of electrospun PAN/PMMA membrane and 1 mol kg^{-1} lithium bis(trifluoromethylsulfonyl)imide in *N*-methyl-*N*-butylpiperidinium bis(trifluoromethanesulfonyl)imide ($PPR_{14}TFSI$) and poly (ethylene glycol) dimethyl ether (PEGDME). The membrane and cell performances are investigated by scanning electron spectroscopy, cyclic voltammetry and electrochemical impedance spectroscopy. It is found that the cell using the GPE based on PAN/PMMA membrane and $PPR_{14}TFSI$-PEGDME (1:1) exhibits the largest discharge capacity and the best cycle durability. The discharge capacity of this cell remains at 760 mA h g^{-1} after 50 cycles. This new sulfur/electrolyte system combines the advantages of the carbon nanofibers that provide an effective conduction path and network-like structure, and the GPE that suppresses the dissolution of the intermediate products generated during the discharge process. The ratio of $PPR_{14}TFSI$ to PEGDME affects the ionic conductivity of the GPE, the stability of the sulfur electrode and the compatibility of lithium electrode with the GPE.

1. Introduction

The high-energy density lithium ion rechargeable batteries are developed as important power sources for clean and efficient energy storage and conversion technologies, especially for electric vehicles (EVs) and hybrid electric vehicles (HEVs) [1–4]. The lithium-sulfur redox couple has a theoretical specific capacity of 1675 mA h g^{-1} and the theoretical specific energy of a lithium-sulfur is 2600 Wh kg^{-1} on the assumption of the complete reaction of lithium with sulfur to Li_2S. Therefore, sulfur is a promising positive active material for high-energy-density batteries [5–13]. Although the lithium-sulfur battery has high specific capacity, it is impossible to discharge fully a battery with such cathode because of the highly electrical insulating nature of sulfur and the high solubility of lithium polysulfides as intermediate products generated during the discharge process in traditional organic liquid electrolyte [14–17].

In order to solve these problems, on the one hand, researchers focus on finding appropriate carbon/sulfur composite materials instead of elemental sulfur to improve the utilization of sulfur and the cycle durability of the cathode. Carbon is not only acted as electrical conductor but also supplied electrochemical reaction sites for sulfur [18–21]. As reported in Ref. [20], the carbon in the composite is electrochemically inactive but serves as the electronic conductor and provides electrochemical reaction interface, which is important for the improvement of rate performance and sulfur utilization. Moreover, linear carbon materials (such as carbon nanotube) were used to prepare carbon/sulfur composite cathode materials. They provide an effective conduction path and network-like structure that can maintain a structural stability of sulfur cathode during discharge–charge process [22–25].

On the other hand, researchers focus on finding appropriate electrolyte to replace the traditional organic liquid electrolyte systems that are composed of carbonates and lithium salt. The traditional liquid electrolyte causes the deterioration in battery performance due to the dissolution of polysulfide. All solid state electrolyte (such as Li_2S–P_2S_5 glass–ceramic) is an ideal solution to the dissolution of polysulfide, but solid state electrolyte has low ionic conductivity, about two decades lower than that of liquid

* Corresponding author. School of Chemistry and Environment, South China Normal University, Guangzhou 510006, China. Tel./fax: +86 20 39310256.
E-mail address: liwsh@scnu.edu.cn (W. Li).

0378-7753/$ – see front matter © 2012 Elsevier B.V. All rights reserved.
doi:10.1016/j.jpowsour.2012.03.111

electrolyte, and therefore is not suitable for the application in a practical battery [26]. Alternatively, gel polymer electrolyte, using polymer matrix to immobilize the liquid electrolyte, has its ionic conductivity close to liquid electrolyte, and is found to be able to decrease the solubility of lithium polysulfides for lithium-sulfur battery [27].

Ionic liquids (ILs) have been the main focus of many recent scientific investigations, due to their unique physical and chemical properties, such as non-volatile, non-flammable, and miscible with a number of organic solvents. From an electrochemical point of view, ILs, offering a high ionic conductivity and a wide potential window, can be used as excellent electrolytes. For these reasons, ILs have attracted much attention for their potential application to electrochemical capacitors or non-aqueous batteries [17,28–32].

In this work, we reported a novel lithium-sulfur cell system, a carbon nanofiber–sulfur composite (CNFs–S) cathode material combined with gel polymer electrolyte. The carbon nanofibers supply electrochemical reaction sites for sulfur and provide an effective conduction path for sulfur cathode. The gel polymer electrolyte, consisting of electrospun poly(acrylonitrile)/poly-(methyl methacrylate) (PAN/PMMA) membrane and 1 mol kg^{-1} lithium bis(trifluoromethylsulfonyl)imide (LiTFSI) in *N*-methyl-*N*-butylpiperidinium bis(trifluoromethanesulfonyl)imide ($PPR_{14}TFSI$) and poly (ethylene glycol) dimethyl ether (PEGDME), reduces the solubility of lithium polysulfides for lithium-sulfur battery. The combined effect of the carbon nanofiber–sulfur composite cathode and gel polymer electrolyte is expected to improve the performance of lithium/sulfur cell.

2. Experimental

2.1. Preparation of CNFs–S composites and sulfur cathode

10 wt% Poly(acrylonitrile) (PAN) and poly(L-lactic acid) (PLLA) (PAN:PLLA = 8:2, by weight) was dissolved in 90 wt% *N*,*N*-dimethylformamide (DMF) under mechanical stirring for at least 24 h to obtain a homogeneous solution. A variable high-voltage power supply (Gamma ES40P-20 W/DAM) was used to provide a high-voltage (around 15 kV) for electrospinning. Then, the electrospun PAN/PLLA nanofiber was carbonized to form carbon nanofibers (CNFs). The CNFs–S composite was synthesized by chemical deposition method in an aqueous solution as reported in our previous work [33]. The CNFs–S electrode was composed of 70 wt% of CNFs–S, 20 wt% Super-P carbon, 10 wt% carboxyl methyl cellulose (CMC) and styrene butadiene rubber (SBR)(CMC:SBR = 2:3, by weight) and the sulfur electrode for comparison was composed of 50 wt% pure sulfur, 40 wt% Super-P carbon and 10 wt% of CMC + SBR.

2.2. Preparation of gel polymer electrolyte

10 wt% (by weight) homogeneous solution of PAN and PMMA (4:1, by ratio) was prepared in DMF under mechanical stirring for 24 h at 60 °C [34,35]. PAN/PMMA fibrous membranes were prepared by electrospinning at room temperature. The electrospinning provides membrane with better porosity that is important for the GPE formation and performance improvement. The GPEs were prepared by immersing the electrospun PAN/PMMA membrane in 1 mol kg^{-1} LiTFSI in $PPR_{14}TFSI$ or 1 mol kg^{-1} LiTFSI in $PPR_{14}TFSI$ + PEGDME ($PPR_{14}TFSI$: PEGDME = 2:1, 1:1 and 1:2, by weight) for 2 h. PEGDME (M_w = 250), $PPR_{14}TFSI$ and LiTFSI were purchased from Aldrich–Sigma and used without further treatment.

2.3. Characterization and measurements

The morphology of the samples was investigated by using scanning electron microscope (JEOL, JSM-6380LV, Japan) coupled with an energy-dispersive X-ray spectrometer (EDX). Sulfur ratio in composite was ascertained by thermogravimetric analyzer (NETZSCH STA 409 PC/PG). CR2032-type coin cell was set up by using the prepared GPEs as the electrolyte. Electrochemical impedance spectrum was obtained with Solartron 1287 ECI, from 10 kHz to 100 mHz at amplitude of ±5 mV. Cyclic voltammetry was conducted using a Princeton PAR273A potentiostat at a scan rate of 0.05 mV s^{-1}. The discharge–charge tests were carried out with Arbin battery cycler (BT-2000) at 0.1C. All of the capacity values in this article are calculated based on the mass of active material S.

3. Results and discussion

3.1. SEM, EDX and TGA of CNFs–S composite material

Fig. 1 shows the morphological characterization of CNFs and CNFs–S composite. It can be seen from the inset of Fig. 1 (a) that the CNFs is porous. While sulfur is precipitating from aqueous solution, CNFs serve as the support and sulfur deposits on CNFs surface and grows up to wrap the whole CNFs, as shown in Fig. 1 (b). The sulfur coating can be identified, as indicated by the arrows in the inset of Fig. 1 (b). The energy-dispersive X-ray (EDX) microanalysis in Fig. 1 (c) confirms the existence of S in the CNFs–S composites. As indicated in the thermogravimetric analysis (TGA) in Fig. 1 (d), about 70 wt% S is coated on the CNFs. This core–shell structure of CNFs–S is beneficial for the improvement of the capacity and the cycle life of lithium-sulfur cell, because it has a sturdier three-dimensional carbon network matrix that provides a good electronic conductivity and accommodates the mechanical stress induced by volume change caused by the redox reaction of sulfur during the discharge–charge cycles.

3.2. SEM of GPEs

Fig. 2 shows the SEM images of electrospun PAN/PMMA membrane before and after gelatinization. The gelatinization is accomplished by immersing the electrospun PAN/PMMA membrane in the ionic liquid based electrolytes for 2 h and then gently removing any excessive liquid using a paper tissue. From the Fig. 2 (a), it can be seen clearly that the electrospun PAN/PMMA membrane has a three-dimensional network of interlaid fibers, which not only imparts sufficient mechanical strength to the membrane, but also generates a porous structure in the membrane. The fully-interconnected micron-sized pores in the membrane favor the preparation of gel polymers. After electrolyte absorption, as seen in Fig. 2 (b, c, d, e), the electrospun PAN/PMMA membranes become largely swollen and more entangled. The fibers are in closer contact to each other with the fibrous structure still retained. The overall pictures clearly show extensive interaction between the fibers and the electrolyte. It can be noted that the interaction is affected by the PEGDME content. The interconnected pore structure can be identified for the membrane with the ratio of $PPR_{14}TFSI$ to PEGDME equal to 1:1 (by weight), as shown in Fig. 2 (d). The dependence of the interaction on the PEGDME content can be ascribed to the viscosity of the electrolyte. The viscosity of $PPR_{14}TFSI$ favors its incorporation in the membrane. The addition of PEGDME reduces the viscosity of $PYR_{14}TFSI$ [36], which accounts for the poor incorporation of the electrolyte in the membrane when increasing the PEGDME content. High viscosity does not favor the ion transportation, while low viscosity does not favor the incorporation of electrolyte in membrane. Therefore, proper ratio of

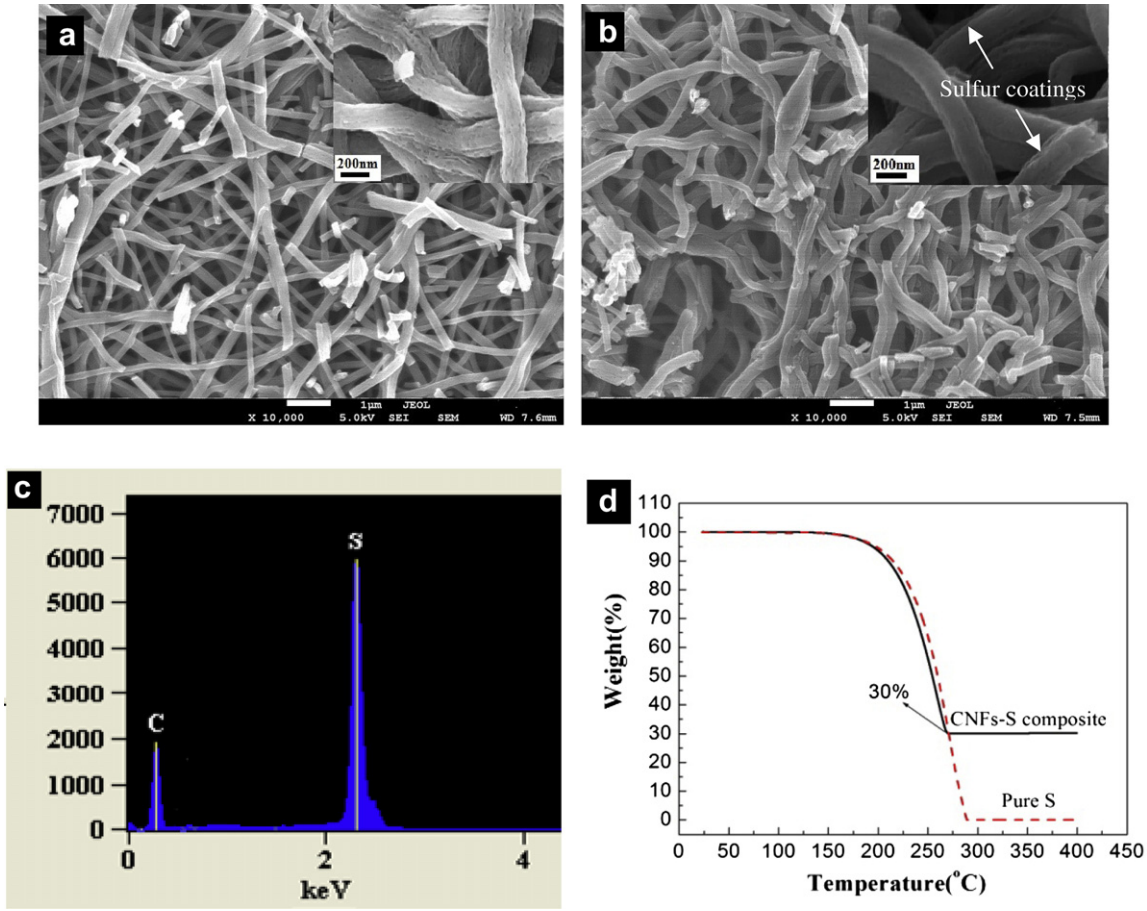

Fig. 1. SEM micrographs of the CNFs (a), CNFs–S composite (b); EDX spectrum of CNFs–S composite (c); TGA curves of CNFs–S composite and pure S (d).

$PPR_{14}TFSI$ to PEGDME is required for the application of this new GPE in lithium-sulfur battery.

3.3. TGA of GPE

The thermal properties of the membranes were determined by TGA. Fig. 3 shows the TGA responses. It can be seen from Fig. 3 (a) that the electrospun PAN/PMMA membrane begins to decompose at about 300 °C but retains about 35% of its primary weight at 600 °C, indicating that PAN/PMMA is stable up to 300 °C and its decomposition involves only the breakdown of partial bonds in its molecule rather than the formation of carbon dioxide even at the temperature higher than 600 °C. Interestingly, the PAN/PMMA membrane incorporating with IL $PPR_{14}TFSI$ begins to decompose at about 350 °C but loses its weight completely at about 480 °C, as shown in Fig. 3 (b). PAN/PMMA with $PPR_{14}TFSI$ is stable up to 350 °C, indicating that the thermal stability of PAN/PMMA can be improved by $PPR_{14}TFSI$. The complete weight loss at 480 °C suggests that $PPR_{14}TFSI$ favors the transformation of the decomposed PAN/PMMA into carbon dioxide. However, thermal stability of the PAN/PMMA membrane decreases when incorporating with IL $PPR_{14}TFSI$ and PEGDME, as shown in Fig. 3 (c, d, e). The electrospun PAN/PMMA membrane with $PPR_{14}TFSI$:PEGDME (2:1, by weight) starts to loose weight about 160 °C. The temperature that the membrane starts to loose weight decreases with increasing the amount of PEGDME, suggesting that the weight loss is caused by the evaporation of the PEGDME. The thermal properties of PAN/PMMA-$PPR_{14}TFSI$-PEGDME mixtures are strongly dependent on the amount of PEGDME and lower PEGDME contents in the mixture result in better thermal properties of the mixture. Similar result was report by Shin et al. [36].

3.4. Electrolyte uptake of membranes and ionic conductivity of GPEs

Table 1 presents electrolyte uptakes of the electrospun PAN/PMMA membranes and conductivities of the corresponding GPEs, which were determined by the methods reported in previous studies [34]. It can be seen from Table 1 that the electrolyte uptake is 680%, 500%, 450% and 280% for electrospun PAN/PMMA membrane with $PPR_{14}TFSI$, $PPR_{14}TFSI$:PEGDME (2:1,by weight), $PPR_{14}TFSI$:PEGDME (1:1, by weight) and $PPR_{14}TFSI$:PEGDME (1:2, by weight), respectively. The absorption of the large amount of liquid electrolyte by the electrospun PAN/PMMA membrane results from the fully-interconnected pore structure and the partial gelation of electrospun PAN/PMMA membranes [37,38]. The difference in electrolyte uptake can be ascribed to the different viscosity of the electrolyte. The electrospun PAN/PMMA membrane for the electrolyte with $PYR_{14}TFSI$ but without PEGDME has the largest electrolyte uptake. This should be ascribed to the high viscosity of IL $PPR_{14}TFSI$. The electrolyte uptake of electrospun PAN/PMMA membrane decreases with increasing the PEGDME content, which is in agreement with the SEM observation from Fig. 2.

The ionic conductivity of the GPEs at 25 °C was determined by the electrochemical impedance spectroscopy as reported in reference [34]. The obtained ionic conductivity is presented in Table 1. As can be seen from Table 1, the GPE with $PPR_{14}TFSI$ but without PEGDME has the lowest conductivity, although the corresponding

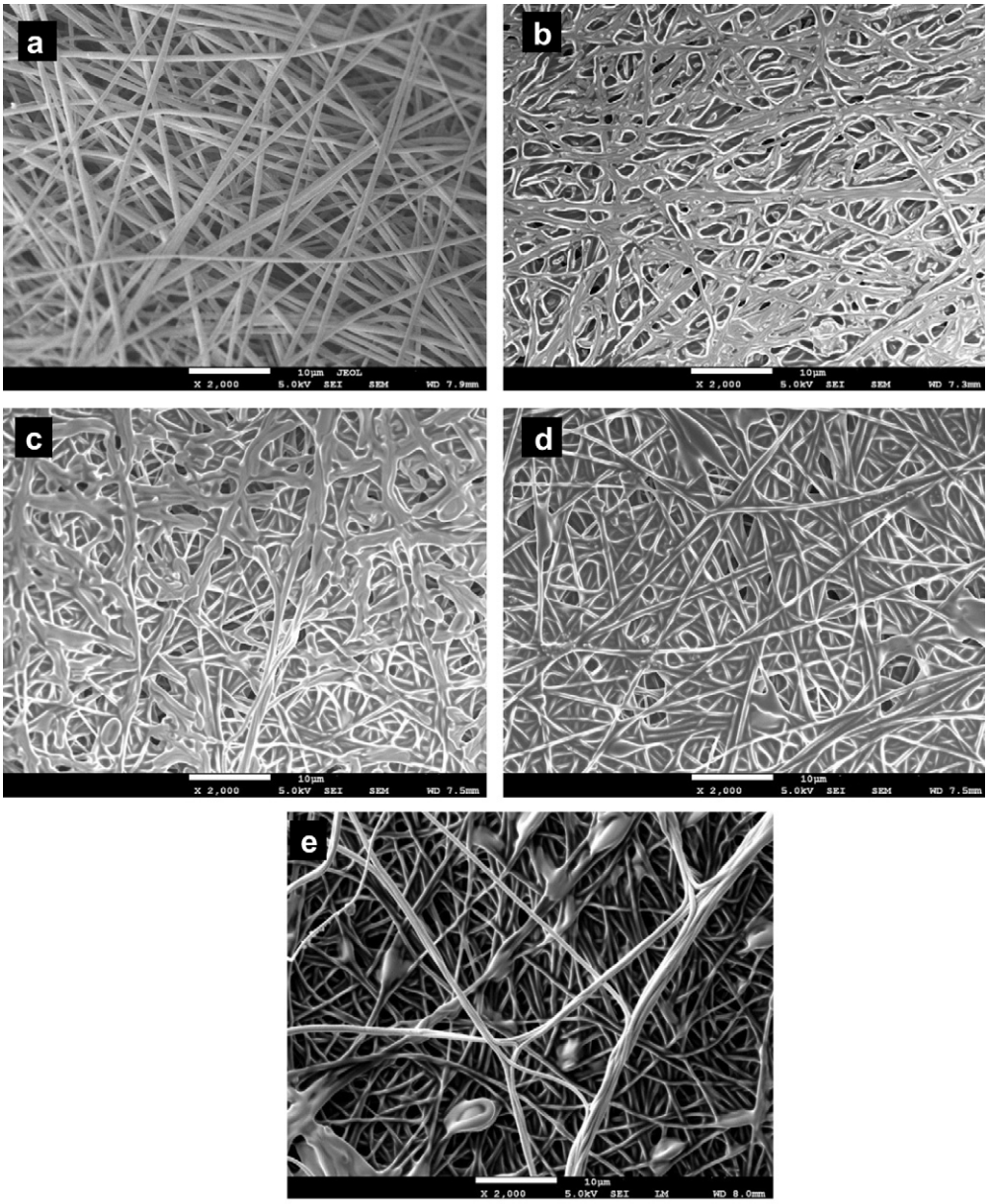

Fig. 2. SEM micrographs of electrospun PAN/PMMA membrane before (a) and after electrolyte uptake: (b) $PPR_{14}TFSI$; (c) $PPR_{14}TFSI$:PEGDME (2:1, by weight); (d) $PPR_{14}TFSI$:PEGDME (1:1, by weight) and (e) $PPR_{14}TFSI$:PEGDME (1:2, by weight).

membrane has the largest electrolyte uptake. Apparently, the high viscosity of $PYR_{14}TFSI$ does not favor the ionic transportation. For the GPEs with PEGDME, the ionic conductivity is not proportional to the electrolyte uptake, and the GPE with $PPR_{14}TFSI$:PEGDME = 1:1 has the highest ionic conductivity. This suggests that the ionic conductivity of the GPE is related not only to the viscosity of the electrolyte but also to the IL $PPR_{14}TFSI$ concentration in the electrolyte.

3.5. Compatibility of GPEs with lithium

The initial impedance behaviors of the cell Li/GPE/Li are presented in Fig. 4. All the impedance spectra are composed by a semicircle at high frequencies, which is related to the contact resistance and charge transfer resistance, and a short inclined line in low frequency regions, which is related to the ion diffusion [39]. The diameter of the semicircle reflects electrode/electrolyte interfacial resistance, which determines interfacial stability and the cyclic stability of lithium battery [40–42]. The initial interfacial resistance is 500, 160, 108, 100 Ω for electrospun PAN/PMMA membranes with $PPR_{14}TFSI$, $PPR_{14}TFSI$:PEGDME (2:1, by weight), $PPR_{14}TFSI$:PEGDME (1:1, by weight) and $PPR_{14}TFSI$:PEGDME (1:2, by weight), respectively. The interfacial resistance is largest for the membrane with $PPR_{14}TFSI$ but without PEGDME, suggesting that there is a poor compatibility between lithium and the GPE containing only IL $PPR_{14}TFSI$. With the incorporation of PEGDME, the interfacial resistance becomes smaller and decreases with increasing the PEGDME content. Fig. 5 presents a comparison of the interfacial resistance of Li/GPE/Li and Li/GPE/CNFs–S cells using the same GPE. The Li/GPE/Li always shows larger interfacial resistance than the Li/GPE/CNFs–S cell, suggesting that the lithium anode contributes mainly to the interfacial resistance of lithium/sulfur cell

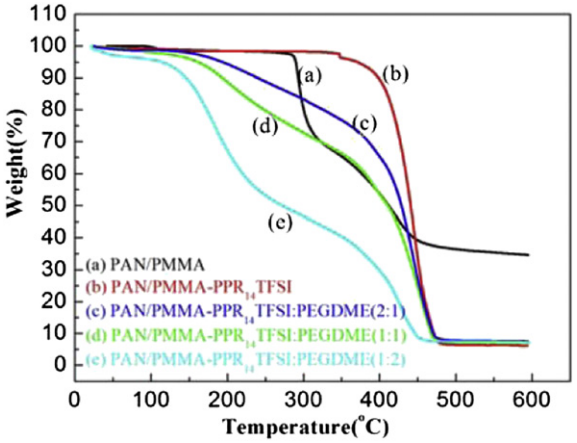

Fig. 3. TGA curves for membrane PAN/PMMA, PAN/PMMA with $PPR_{14}TFSI$, PAN/PMMA with $PPR_{14}TFSI$:PEGDME (2:1, by weight), PAN/PMMA with $PPR_{14}TFSI$:PEGDME (1:1, by weight) and PAN/PMMA with $PPR_{14}TFSI$:PEGDME (1:2, by weight) from room temperature to 600 °C at a heating rate of 5 °C min^{-1} under Ar atmosphere.

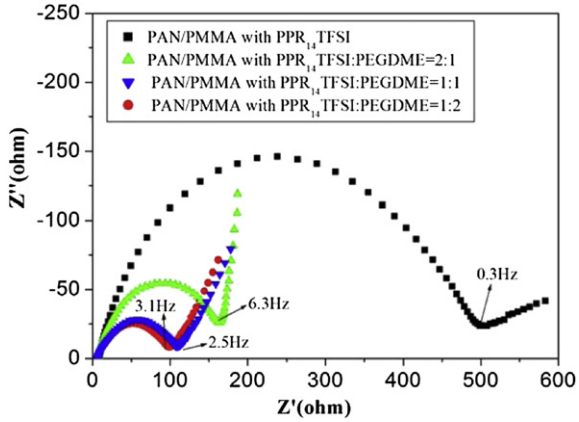

Fig. 4. Nyquist plots of Li/GPE/Li cells using different GPEs (a) PAN/PMMA with $PPR_{14}TFSI$; (b) PAN/PMMA with $PPR_{14}TFSI$:PEGDME (2:1, by weight); (c) PAN/PMMA with $PPR_{14}TFSI$:PEGDME (1:1, by weight) and (d) PAN/PMMA with $PPR_{14}TFSI$:PEGDME (1:2, by weight), frequency range: 100 kHz–10 mHz.

more than the sulfur cathode. It is obvious that PEGDME can improve the compatibility of IL $PYR_{14}TFSI$ based GPE with lithium electrode. Therefore, the battery using the GPE based on electrospun PAN/PMMA membrane with IL $PPR_{14}TFSI$ and PEGDME can be expected to exhibits good performance.

3.6. Stability of CNFs–S/GPE system

Fig. 6 shows cyclic voltammograms of lithium-sulfur cells combining CNFs–S cathode and GPE. All the voltammograms show one or two oxidation and reduction peak potential. The reduction peaks between 2.0 V and 2.5 V are related to the change from elemental sulfur to the higher-order lithium polysulfides (Li_2S_n, $n \geq 4$), the reduction peaks between 1.5 V and 2.0 V are related to the reduction of higher-order lithium polysulfides to lower-order lithium polysulfides (Li_2S_n, $n < 4$) and lithium sulfide [12,13,16,21]. It can be seen from Fig. 6(a) that the battery using the GPE with $PPR_{14}TFSI$ but without PEGDME shows broad oxidation peaks at about 2.7 V and reduction peaks at about 2.2 V and 1.7 V, but a small reduction peak at about 2.2 V. The peak current increases with cycles in the first three cycles and keeps unchanged in the latter cycles, suggesting that the CNFs–S electrode is stable when it contacts to the GPE containing only IL $PPR_{14}TFSI$. When incorporating with PEGDME, the batteries show a clearer reduction peak at about 2.2 V, but broader reduction peak at about 1.6 V, as shown by Fig. 6 (b, c and d), suggesting that PEGDME affect the electrode process. It can be noted from the variation of peak current with cycle that the battery using IL $PPR_{14}TFSI$ based GPE ($PPR_{14}TFSI$:PEGDME = 1:1) has the best stability among the GPEs with different contents of PEGDME. The narrow but high profile of the main reduction peak reveals sulfur in the CNFs–S composite has a low inner resistance.

The battery using the GPE ($PPR_{14}TFSI$:PEGDME = 1:2) also reveals sharp reduction peaks at about 2.6 V and reduction peaks at 2.45 V and 1.9 V in the first cycle, as shown by Fig. 6(d). However, the peak current decreases with cycle significantly, suggesting that the sulfur electrode is unstable in this case. The less stability of sulfur contacting to the GPE with high PEGDME can be ascribed to the lower viscosity of the electrolyte that favors the dissolution of the polysulfides into the electrolyte during the discharge/charge process.

It can be inferred from the results above that the IL $PPR_{14}TFSI$ suppresses effectively the dissolution of the polysulfides into the electrolyte during the discharge/charge process, but its high viscosity does not favor the ionic transportation. Incorporating appropriate PEGDME can decrease the viscosity of the IL $PPR_{14}TFSI$ and thus improve the battery performance.

Table 1
Electrolyte uptake of electrospun P(AN–MMA) membrane and conductivity of corresponding GPEs. (1 M kg^{-1} LiTFSI in $PPR_{14}TFSI$ or 1 M kg^{-1} LiTFSI in $PPR_{14}TFSI$ + PEGDME) ($PPR_{14}TFSI$:PEGDME = 2:1, 1:1 and 1:2, by weight).

$PPR_{14}TFSI$:PEGDME (by weight)	1:0	2:1	1:1	1:2
Uptake (wt%)	680	500	450	280
Conductivity (× 10^{-3} S cm^{-1})	1.1	2.4	3.8	2.8

3.7. Performance of Li/S cell

Fig. 7 shows the cycle stability of CNFs–S cathode with different GPEs. It can be seen from Fig. 7 that the battery using the IL $PPR_{14}TFSI$ based GPE with PEGDME shows better cycle performance than the battery using the GPE without PEGDME. The initial discharge capacity at 0.15 mA cm^{-2} is 560, 1148, 1200, 1150 mA h g^{-1} for electrospun PAN/PMMA membranes with $PPR_{14}TFSI$, $PPR_{14}TFSI$:PEGDME (2:1, by weight), $PPR_{14}TFSI$:PEGDME (1:1, by weight) and $PPR_{14}TFSI$:PEGDME (1:2, by weight), respectively. Fig. 8 presents their initial discharge–charge curves. In the

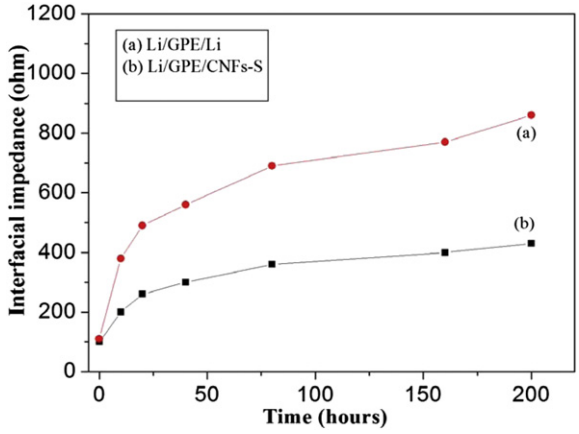

Fig. 5. Interfacial impedance evolution of Li/GPE/Li and Li/GPE/CNFs–S cells using the GPE PAN/PMMA with $PPR_{14}TFSI$:PEGDME (1:1, by weight).

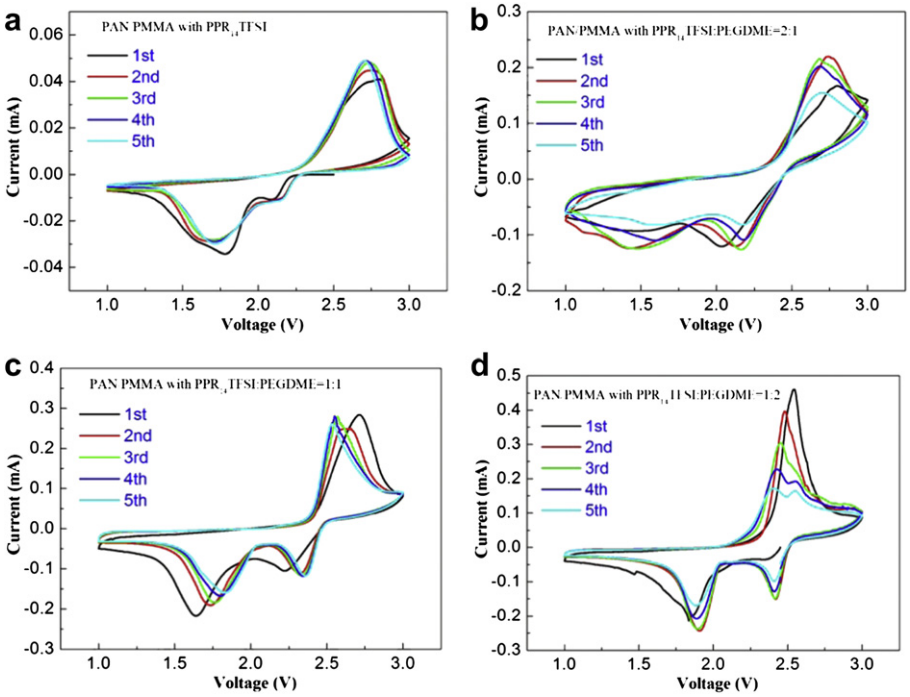

Fig. 6. Cyclic voltammograms of lithium-sulfur cells with CNFs–S cathode and different GPEs (a) PAN/PMMA with $PPR_{14}TFSI$; (b) PAN/PMMA with $PPR_{14}TFSI$:PEGDME (2:1, by weight); (c) PAN/PMMA with $PPR_{14}TFSI$:PEGDME (1:1, by weight) and (d) PAN/PMMA with $PPR_{14}TFSI$:PEGDME (1:2, by weight), at scan range: 1.0–3.0 V; scan rate: 0.05 mV s^{-1}.

case of $PPR_{14}TFSI$ based GPE without PEGDME, the initial discharge capacity is very low, only 560 mA h g^{-1}, increases gradually to about 1000 mA h g^{-1} in the first several cycles, decreases drastically with increasing cycle number, and remains only 400 mA h g^{-1} after 50 cycles. This can be ascribed to the high viscosity of $PPR_{14}TFS$ and the poor compatibility of lithium electrode with the GPE with only IL. Due to the high viscosity of $PPR_{14}TFSI$, the cathode is not easy to wet by the electrolyte leading to the low initial capacity, and the poor compatibility of lithium electrode with the GPE accounts for decreasing capacity in the latter cycles.

The battery using the GPE with $PPR_{14}TFSI$:PEGDME = 1:1 (by weight) exhibits the best performance. The discharge capacity of the battery remains 760 mA h g^{-1} after 50 cycles at 0.15 mA cm^{-2}. This performance can be ascribed to the highest ionic conductivity of this GPE, the best stability of CNFs–S electrode and better compatibility of lithium electrode with this GPE. For comparison, the sulfur electrode was prepared and tested with electrospun PAN/PMMA membrane with $PPR_{14}TFSI$:PEGDME = 1:1 (by weight). By comparing Fig. 7 (c) with Fig. 7 (e), it can be seen that the CNFs–S cathode has larger discharge capacity and better cycle performance than the sulfur electrode. It is obvious that the combination of the core–shell structure of CNFs–S composite and the GPE with appropriate ratio of $PPR_{14}TFSI$ to PEGDME provides a solution to the performance improvement of lithium-sulfur battery.

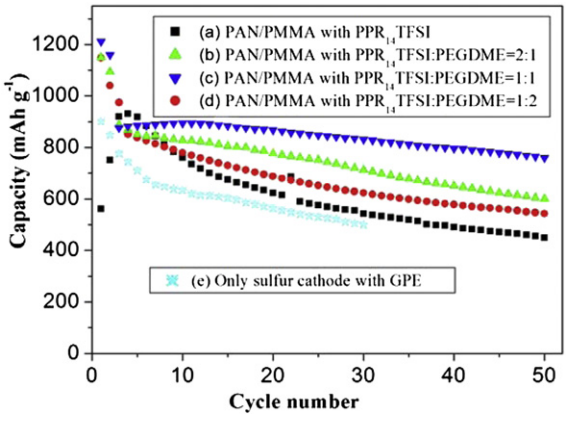

Fig. 7. Cyclability of lithium-sulfur cells with CNFs–S cathode and different GPEs (a) PAN/PMMA with $PPR_{14}TFSI$; (b) PAN/PMMA with $PPR_{14}TFSI$:PEGDME (2:1, by weight); (c) PAN/PMMA–$PPR_{14}TFSI$:PEGDME (1:1, by weight); (d) PAN/PMMA with $PPR_{14}TFSI$:PEGDME (1:2, by weight); (e) The sulfur electrode from a mixture of 50 wt% of S, 40 wt% of Super-P carbon, 10 wt% CMC + SBR with PAN/PMMA–$PPR_{14}TFSI$:PEGDME (1:1, by weight). Discharge rate: 0.15 mA cm^{-2}, after an initial activation processes at 0.03 mA cm^{-2} for 2 cycles, active area of electrodes: sulfur cathode (0.9 cm^2), Li anode (1.6 cm^2); loading of active material: 0.8 mg.

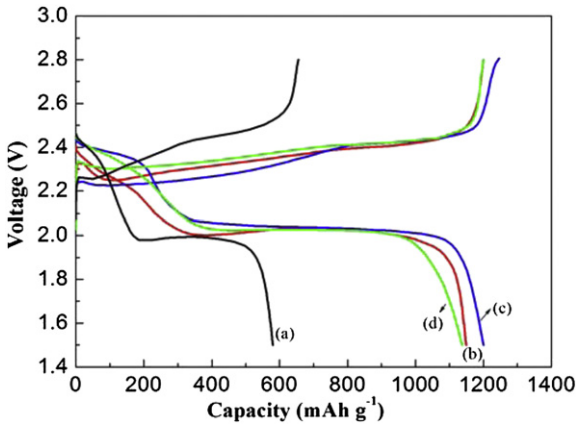

Fig. 8. Discharge and charge curves of lithium-sulfur cells with CNFs–S cathode and different GPEs (a) PAN/PMMA with $PPR_{14}TFSI$; (b) PAN/PMMA with $PPR_{14}TFSI$:PEGDME (2:1, by weight); (c) PAN/PMMA with $PPR_{14}TFSI$:PEGDME (1:1, by weight) and (d) PAN/PMMA with $PPR_{14}TFSI$:PEGDME (1:2, by weight). Discharge and charge rate: 0.03 mA cm^{-2}, active area of electrodes: sulfur cathode (0.9 cm^2), Li anode (1.6 cm^2); loading of active material: 0.8 mg.

4. Conclusions

The results reported in this paper demonstrate the relevance of carbon nanofiber–sulfur cathode material and gel polymer electrolyte for the development of high-energy lithium-sulfur cell. The lithium-sulfur cell exhibits excellent performance with a unique combination of carbon nanofiber–sulfur electrode and gel polymer electrolyte based on PAN/PMMA membrane and $PPR_{14}TFSI$–PEGDME (1:1, by weight) electrolyte. This ratio of $PPR_{14}TFSI$ to PEGDME yields the highest ionic conductivity of GPE, the best stability of the sulfur and the appropriate compatibility of lithium electrode with the GPE.

Acknowledgements

The authors are highly grateful for the financial support from the joint project of National Natural Science Foundation of China and Natural Science Foundation of Guangdong Province (Grant No. U1134002), Combination Project of Enterprise, University and Scientific Research of Guangdong Province (Grant No. 2010A010200001) and Natural Science Foundation of Guangdong Province (Grant No. 10351063101000001).

References

[1] E.J. Cairns, P. Albertus, Annu. Rev. Chem. Biomol. Eng. 1 (2010) 299–320.
[2] M.S. Whittingham, Chem. Rev. 104 (2004) 4271–4302.
[3] T. Tabuchi, N. Hochgatterer, Z. Ogumi, M. Winter, J. Power Sources 188 (2009) 552–557.
[4] T. Tabuchi, Y. Katayama, T. Nukuda, Z. Ogumi, J. Power Sources 191 (2009) 640–643.
[5] H. Yamin, E. Peled, J. Power Sources 9 (1983) 281–287.
[6] H. Yamin, J. Penciner, A. Gorenshtain, M. Elam, E. Peled, J. Power Sources 14 (1985) 129–134.
[7] H. Yamin, A. Gorenshtein, J. Penciner, Y. Sternberg, E. Peled, J. Electrochem. Soc. 135 (1988) 1045–1048.
[8] E. Peled, A. Gorenshtein, M. Segal, Y. Sternberg, J. Power Sources 26 (1989) 269–271.
[9] E. Peled, T. Sternberg, A. Gorenshtein, Y. Lavi, J. Electrochem. Soc. 136 (1989) 1621–1625.
[10] X. Ji, K.T. Lee, L.F. Nazar, Nat. Mater. 8 (2009) 500–506.
[11] N. Jayaprakash, J. Shen, S.S. Moganty, A. Corona, L.A. Archer, Angew. Chem. Int. Ed. 50 (2011) 5904–5908.
[12] L. Ji, M. Rao, H. Zheng, L. Zhang, Y. Li, W. Duan, J. Guo, E.J. Cairns, Y. Zhang, J. Am. Chem. Soc. 133 (2011) 18522–18525.
[13] L. Ji, M. Rao, S. Aloni, L. Wang, E.J. Cairns, Y. Zhang, Energy Environ. Sci. 4 (2011) 5053–5059.
[14] S.E. Cheon, S.S. Choi, J.S. Han, Y.S. Choi, B.H. Jung, H.S. Lim, J. Electrochem. Soc. 151 (2004) A2067–A2073.
[15] S. Li, M. Xie, J. Liu, H. Wang, H. Yan, Electrochem. Solid State Lett. 14 (2011) A105–A107.
[16] J. Shim, K.A. Striebel, E.J. Cairns, J. Electrochem. Soc. 149 (2002) A1321–A1325.
[17] L.X. Yuan, J.K. Feng, X.P. Ai, Y.L. Cao, S.L. Chen, H.X. Yang, Electrochem. Commun. 8 (2006) 610–614.
[18] S. Wei, H. Zhang, Y. Huang, W. Wang, Y. Xia, Z. Yu, Energy Environ. Sci. 4 (2011) 736–740.
[19] C. Wang, J. Chen, Y. Shi, M. Zheng, Q. Dong, Electrochim. Acta 55 (2010) 7010–7015.
[20] C. Liang, N.J. Dudney, J.Y. Howe, Chem. Mater. 21 (2009) 4724–4730.
[21] Y. Cao, X. Li, I.A. Aksay, J. Lemmon, Z. Nie, Z. Yang, J. Liu, Phys. Chem. Chem. Phys. 13 (2011) 7660–7665.
[22] J. Chen, X. Jia, Q. She, C. Wang, Q. Zhang, M. Zheng, Q. Dong, Electrochim. Acta 55 (2010) 8062–8066.
[23] L. Yin, J. Wang, J. Yang, Y. Nuli, J. Mater. Chem. 21 (2011) 6807–6810.
[24] L. Yuan, H. Yuan, X. Qiu, L. Chen, W. Zhu, J. Power Sources 189 (2009) 1141–1146.
[25] W. Wei, J. Wang, L. Zhou, J. Yang, B. Schumann, Y. NuLi, Electrochem. Commun. 13 (2011) 399–402.
[26] M. Nagao, A. Hayashi, M. Tatsumisago, Electrochim. Acta 56 (2011) 6055–6059.
[27] D. Marmorstein, T.H. Yu, K.A. Striebel, F.R. McLarnon, J. Hou, E.J. Cairns, J. Power Sources 89 (2000) 219–226.
[28] L. Damen, M. Lazzari, M. Mastragostino, J. Power Sources 196 (2011) 8692–8695.
[29] S. Fang, Y. Jin, L. Yang, S. Hirano, K. Tachibana, S. Katayama, Electrochim. Acta 56 (2011) 4663–4671.
[30] J.H. Shin, E.J. Cairns, J. Electrochem. Soc. 155 (2008) A368–A373.
[31] S. Fang, Y. Tang, X. Tai, L. Yang, K. Tachibana, K. Kamijima, J. Power Sources 196 (2011) 1433–1441.
[32] G.B. Appetecchi, G.T. Kim, M. Montanino, F. Alessandrini, S. Passerini, J. Power Sources 196 (2011) 6703–6709.
[33] M. Rao, W. Li, E.J. Cairns, Electrochem. Commun. 17 (2012) 1–5.
[34] M.M. Rao, J.S. Liu, W.S. Li, Y. Liang, D.Y. Zhou, J. Membr. Sci. 322 (2008) 314–319.
[35] D.Y. Zhou, G.Z. Wang, W.S. Li, G.L. Li, C.L. Tan, M.M. Rao, Y.H. Liao, J. Power Sources 184 (2008) 477–480.
[36] J.H. Shin, E.J. Cairns, J. Power Sources 177 (2008) 537–545.
[37] Q. Xiao, Z. Li, D. Gao, H. Zhang, J. Membr. Sci. 326 (2009) 260–264.
[38] A.M.M. Ali, M.Z.A. Yahya, H. Bahron, R.H.Y. Subban, M.K. Harun, I. Atan, Mater. Lett. 61 (2007) 2026–2029.
[39] Y.J. Choi, Y.D. Chung, C.Y. Baek, K.W. Kima, H.J. Ahn, J.H. Ahn, J. Power Sources 184 (2008) 548–552.
[40] C.S. Kim, S.M. Oh, Electrochim. Acta 46 (2001) 1323–1331.
[41] Y.G. Lee, J.K. Park, S.I. Moon, Electrochim. Acta 46 (2000) 533–539.
[42] N.S. Choi, Y.M. Lee, J.H. Park, J.K. Park, J. Power Sources 119–121 (2003) 610–616.